

Tailored conductivity behavior in nanocrystalline nickel ferrite

Babita Baruwati, K. Madhusudan Reddy, and Sunkara V. Manorama^{a)}
Nanomaterials Laboratory, Indian Institute of Chemical Technology, Hyderabad 500 007, India

Rajnish K. Singh and Om Parkash
*Department of Ceramic Engineering, Institute of Technology, Banaras Hindu University,
 Varanasi 221 005, India*

(Received 21 January 2004; accepted 9 August 2004)

In this letter, we report an important issue in nanoparticle synthesis by the “bottom up” approach. By controlling the pH of the starting mixture of the salts we have been successful in obtaining the desired conductivity of nanosized nickel ferrite. X-ray diffraction and transmission electron microscopy confirmed the size, structure, and morphology of the nanoferrites. All the materials are typical semiconducting oxides whose conductivity depends on the pH of the starting salt solution. Direct current and alternating current conductivity studies coupled with thermoelectric measurements and the resultant activation energies help us to propose the mechanism of conductivity in these ferrites. X-ray photoelectron spectroscopy studies are indicative of Ni^{3+} presence in p -type ferrite. The n - and p -type conductivity in these materials is attributed to the hopping due to the presence of Fe^{3+} and Ni^{3+} ions, respectively. © 2004 American Institute of Physics. [DOI: 10.1063/1.1801685]

Nanoparticles of spinel ferrites, a class of complex oxides, by virtue of their unique electronic or physical structure,¹ display enhanced properties, which may be harnessed for technological applications.^{2,3} Hydrothermal synthesis (HT), a high pressure chemical route that involves a reaction between the constituent ions at elevated temperatures under equilibrium water pressure⁴ has been adopted to obtain pure, homogeneous, and ultrafine oxides in large quantities. Komarneni *et al.*,⁵ obtained single phase ferrites, including nickel ferrite by varying the pH of the starting solution. The electrical conduction, depends to a large extent on the preparation conditions.⁶ Earlier reports exist where composition of the ferrites controlled the transport properties.^{7–9} Hence, there is a thrust in devising synthetic routes to understand the conductivity in these materials. This paper describes the influence of pH of the starting mixture on the structural, electrical conductivity in nanosized $NiFe_2O_4$. HT synthesis of $NiFe_2O_4$ resulted in n -type conductivity when starting solution $pH < 9$ and p type for $pH \geq 9$. A plausible explanation for this tunable conducting behavior is proposed.

X-ray diffraction (XRD) along with transmission electron microscope (TEM) and selected area electron diffraction (SAED) confirmed the structure and morphology while dc and ac conductivity studies coupled with thermoelectric power (TEP) measurements unambiguously established the conduction mechanism in $NiFe_2O_4$. X-ray photoelectron spectroscopy (XPS) study confirms the presence of Ni^{3+} ions in the $NiFe_2O_4$ structure synthesized with initial $pH \geq 9$ supporting the proposed conductivity mechanism.

In a typical reaction, stoichiometric amounts of iron (III) nitrate and nickel (II) nitrate were dissolved in deionized water. The pH of the solution was adjusted to 7 by the addition of aqueous ammonia, stirred vigorously for 2 h and transferred to an autoclave whose temperature was raised to 225 °C and held for 30 min under autogenerated pressure of

20 kg/cm². After cooling, the precipitate was filtered, washed, and dried. The experiment was repeated for pH 8, 9, 10, and 11. The samples obtained would henceforth be referred to as 7, 8, 9, 10, and 11.

XRD confirmed the formation of cubic spinel $NiFe_2O_4$ and the minimum pH for formation of single phase is 7, below which a mixture of $NiFe_2O_4$ and Fe_2O_3 are formed. Crystallite size calculated from the line broadening of (311) Bragg reflection is 9.3 nm and the cubic lattice parameter “ a ” was 8.3 ± 0.02 Å comparable to but lower than the bulk material (8.54 Å). This difference is due to the nanosize of particles which is associated with a large cohesive energy compared to the bulk material.¹⁰ Figure 1 is the TEM micrograph showing nearly spherical particles, along with some agglomerates and the inset shows SAED pattern. Average particle size is ~10–12 nm comparable to the crystallite size calculated from XRD.

A Keithley 236 Source Measure Unit was used to study the current–voltage (I – V) characteristics. Figure 2 shows the log σ versus $1000/T(K)$ plots for $NiFe_2O_4$ nanoparticles ex-

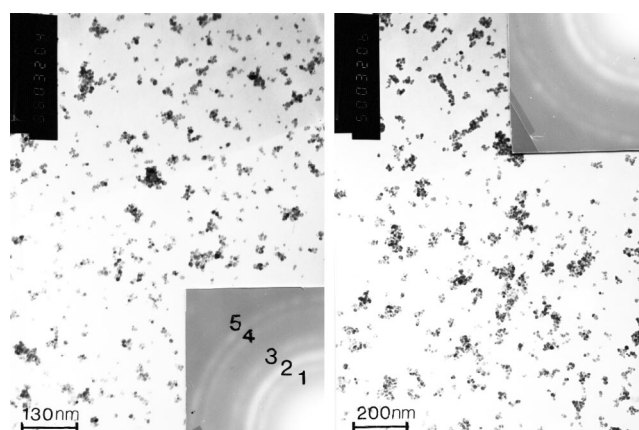


FIG. 1. TEM of the as-prepared nickel ferrite nanoparticles (10–12 nm) and inset shows SAED pattern. Numbers on ring pattern correspond to 220(1), 311(2), 400(3), 511(4), and 440(5) planes.

^{a)}Electronic mail: manorama@iict.res.in

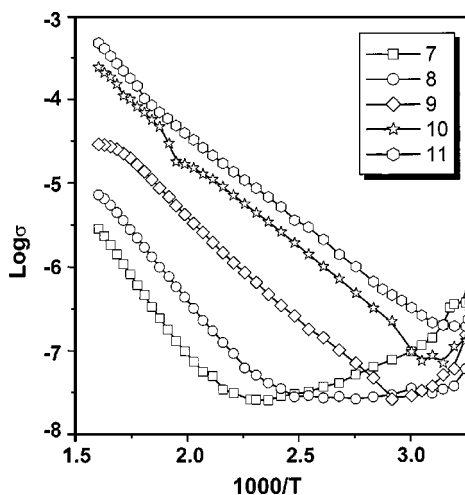


FIG. 2. A typical semiconducting behavior $\log \sigma$ vs $1000/T$ (K)-Arrhenius plot.

hibiting typical semiconducting behavior from which the activation energy, $E_a = k \cdot \text{slope}$ where k is the Boltzmann constant, is estimated. The resulting values of E_a in the range 0.19–0.30 eV, are comparable to earlier reports.¹¹

Initial evidence for the difference in the type of charge carriers came from the response of NiFe_2O_4 to reducing gases. Our earlier studies showed NiFe_2O_4 to be a good sensor for reducing gases.¹² However, as we now report, it is observed that all the NiFe_2O_4 samples do not similarly respond. Samples 7 and 8 show a decrease in resistance ($R_a - R_g$) > 0 , while 9, 10, and 11 show an increase in resistance ($R_a - R_g$) < 0 when exposed to reducing gas. Figure 3(a) shows the plot for ($R_a - R_g$) versus operating temperature, where R_a and R_g are the resistance of sample in air and in presence of liquefied petroleum gas, respectively, showing that samples 7 and 8 behave as n type while 9, 10, and 11 exhibit typical p -type semiconducting behavior.

To elaborate, on these findings TEP measurements were carried out and Table I is a summary of these studies. The Seebeck coefficient is negative for samples 7 and 8 and positive for 9, 10, and 11, establishing that the former are n -type and the latter three p -type semiconductors [Fig. 3(b)], supporting the gas sensing studies. The charge carrier concentrations are calculated using the formula $n = N / [1 + 1/2 \exp(-Se/k)]$, where $N = 10^{22} \text{ cm}^{-3}$ for the low mobility semiconductors having exceedingly narrow bands or localized levels,¹³ S is the Seebeck coefficient and k is the Bolt-

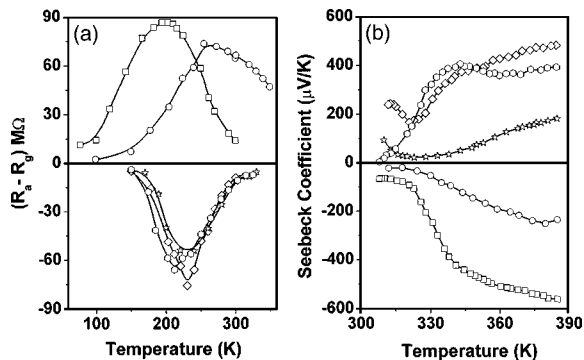


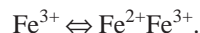
FIG. 3. (a) Change in resistance ($R_a - R_g$) $\text{M}\Omega$ as a function of temperature and, (b) Seebeck coefficient as a function of temperature for samples prepared at pH 7 (\square), 8 (\circ), 9 (\diamond), 10 (\star), and 11 (\circ).

TABLE I. Results from the thermoelectric power measurements on the nanosized NiFe_2O_4 .

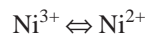
pH	Conductivity type	E_a (eV)	Carrier concentration	Mobility
7	n -	0.30	$\sim 10^{22}$	$\sim 10^{-12}$
8	n -	0.27	$\sim 10^{22}$	$\sim 10^{-12}$
9	p -	0.21	$\sim 10^{19-22}$	$\sim 10^{-(9-11)}$
10	p -	0.19	$\sim 10^{21-22}$	$\sim 10^{-(8-11)}$
11	p -	0.17	$\sim 10^{20-22}$	$\sim 10^{-(8-11)}$

zman constant. In the case of low mobility oxide semiconductors such as ferrites, the activation energies are often associated with the mobility of charge carriers that are considered as localized at the ions or vacant sites and the conduction process occurs via a hopping process. This is supported by the fact that the dc conductivity increases with temperature attributable to the increased thermally activated drift mobility of the charge carriers in accordance with the hopping conduction model. The obtained activation energies ~ 0.2 – 0.3 eV also corroborate with the hopping model and our results also fall in line with earlier reports.¹³

To explain different types of conductivities, we put forth the following argument based on our observations and supporting evidence from literature. The probable reason for the n -type behavior in 7 and 8 is attributed to the presence of Fe^{3+} and the conductivity is predominantly due to hopping of electrons from to Fe^{2+} as follows,



Similarly, p -type conductivity in 9, 10, and 11 is due to the presence of Ni^{3+} and the generation of Ni^{3+} is justified by the high pH maintained during the synthesis. At higher pH the alkaline medium favors NiO formation and thus leads to the minimum necessary condition of obtaining pure NiFe_2O_4 at pH 7. The NiO has an affinity for oxidation forming Ni^{3+} species. Another factor could be the creation of cation vacancies in the ferrite lattice, which form cation (Fe^{3+} + vacancy) complex, that act as p -type carriers. This results in formation of Ni^{3+} species for the overall charge balancing and compensation. The hole conduction is represented as



similar to El-Sayed¹⁴ who also attributes n -type conductivity to the presence of Fe^{3+} and p -type conductivity to the hole transfer from Ni^{3+} to Ni^{2+} ions. The latter behavior is also reported in Ni-Zn ferrites and others where stress contributes to the change in conductivity behavior.^{15,16}

Figures 4(a) and 4(b) depict core level binding energy spectra for the $\text{Ni } 3p_{3/2}$ for sample 7 and 10 respectively. $\text{C } 1s$ at 284.6 eV is taken as reference. The $\text{Ni } 3p_{3/2}$ spectra have been deconvoluted using the Gaussian fitting. Sample 7 shows a single peak at 854.45 eV attributed to Ni^{2+} and sample 10 two peaks at 854.43 due to Ni^{2+} and 855.96 eV due to Ni^{3+} which supports the observed p -type behavior. The binding energies also agree with reported data.^{17,18}

To categorize and assign the contribution of conductivities in these materials due to grain and grain boundaries, ac impedance studies have been carried out from 240°C to room temperature. Figure 5 is the typical impedance plot for sample 10 showing the complex conductivity behavior with two semicircular arcs; a small high frequency arc and a large low frequency arc attributed to conductivity in the grains and

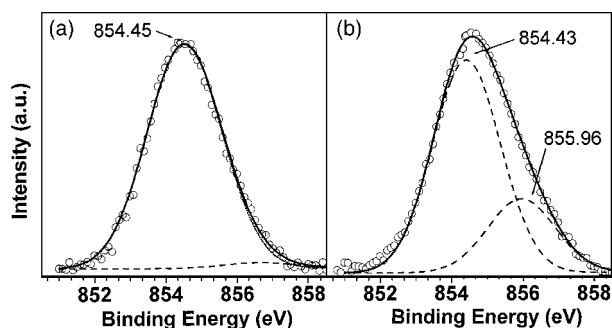


FIG. 4. Ni $3p_{3/2}$ core level XPS spectra for (a) sample 7 and (b) sample 10. Dotted lines represent the Gaussian fits and the circles represent the recorded data.

grain boundaries respectively.¹¹ The corresponding activation energies for the grain and grain boundaries are 0.3 and 0.5 eV of the same order as that obtained from dc conductivity studies.

Following are the inferences drawn from this study:

- (1) We have successfully synthesized nanosized NiFe_2O_4 with desired conductivity by controlling the pH of starting material, n -type at pH 7, 8, and p -type at pH 9, 10, and 11.

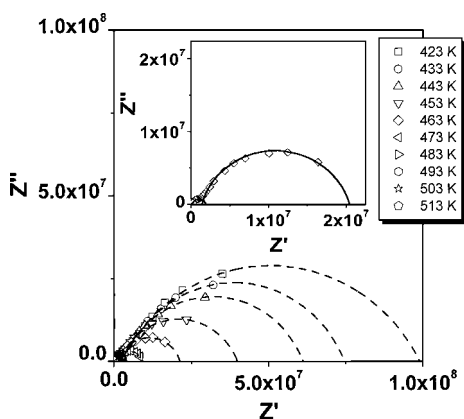


FIG. 5. Typical complex conductivity curve for the sample 10. Inset shows the two well demarcated semicircles. Points represent the data recorded while the solid line is the fitted curve.

- (2) Impedance studies reveal that the conductivity in these ferrites has a contribution both from grains and grain boundaries.
- (3) The activation energy values are indicative of conduction predominantly due to hopping of the carriers namely electrons in the n -type and holes in the p -type Ni ferrite.
- (4) XPS study conclusively establishes the presence of Ni^{3+} in p -type NiFe_2O_4 .

The authors are thankful to Dr. Shashi Singh, CCMB, Hyderabad for her kind cooperation in recording the electron micrographs. B.B. and K.M.R. are thankful to CSIR, New Delhi, India for the Senior Research Fellowship.

¹S. Son, M. Taheri, E. Carpenter, V. G. Harris, and M. E. McHenry, *J. Appl. Phys.* **91**, 7589 (2002).

²M. Sugimoto, *J. Am. Ceram. Soc.* **82**, 269 (1999).

³I. Safarik, and M. Safarikova, *Magnetic Nanoparticles and Biosciences, In Nanostructured Materials*, edited by H. Hofmann, Z. Rahman, and U. Schubert (Springer, Wien, 2002), pp. 1–23.

⁴D. Makovec, M. Drogenik, and A. Znidarsic, *J. Am. Ceram. Soc.* **82**, 1113 (1999).

⁵K. Sridhar, M. C. D'Arrigo, C. Leonelli, G. C. Pellacan, and H. Katsuki, *J. Am. Ceram. Soc.* **81**, 3041 (1998).

⁶M. Guyot, *J. Magn. Magn. Mater.* **18**, 925 (1980).

⁷C. N. Chinnasamy, A. Narayanasamy, N. Ponpandian, K. Chattopadhyay, K. Shinoda, B. Jeyadevan, K. Tohji, K. Nakatsuka, T. Furubayashi, and I. Nakatani, *Phys. Rev. B* **63**, 184108 (2001).

⁸A. Tawfik, *J. Magn. Magn. Mater.* **224**, 197 (2001).

⁹K. Ishino and Y. Naramiya, *Ceram. Bull.* **66**, 1469 (1987).

¹⁰W. H. Qi, M. P. Wang, G. Y. Xu, and J. Y. Chen, in *China-EU Forum on Nanosized Technology*, Beijing, P. R. China., Dec. 2002, p. 86.

¹¹N. Ponpandian, P. Balaya, and A. Narayanasamy, *J. Phys.: Condens. Matter* **14**, 3221 (2002).

¹²L. Satyanarayana, K. Madhusudan Reddy, and S. V. Manorama, *Mater. Chem. Phys.* **82**, 21 (2003).

¹³F. J. Morin, *Phys. Rev.* **93**, 1195 (1953).

¹⁴A. M. El-Sayed, *Mater. Chem. Phys.* **82**, 583 (2003).

¹⁵B. V. Bhise, A. K. Ghatage, B. M. Kulkarni, S. D. Lotke, and S. A. Patil, *Bull. Mater. Sci.* **19**, 527 (1996).

¹⁶D. C. Khan and M. Misra, *Bull. Mater. Sci.* **7**, 253 (1985).

¹⁷M. Aizawa, S. Lee, and S. L. Anderson, *J. Chem. Phys.* **117**, 5001 (2002).

¹⁸C. D. Wagner, W. M. Riggs, L. E. Davis, and J. E. Moulder, in *Handbook of X-Ray Photoelectron Spectroscopy*, edited by G. E. Muilenberg (Perkin-Elmer, Physical Electronics, Eden Prairie, MN, 1979).